


Anisotropic phonon thermal transport in nitrophosphorene monolayer

Armin Taheri and Chandra Veer Singh ^{*}

Department of Materials Science and Engineering, University of Toronto, 184 College St, Toronto, M5S 3E4, Ontario, Canada

 (Received 15 December 2020; revised 9 February 2021; accepted 16 March 2021; published 29 March 2021)

Recent studies have shown that although black phosphorene (α -P) has promising electrical, thermal, and mechanical properties, its poor stability in the air makes its applications challenging. Very recently, monolayer puckered-phase nitrophosphorene (α -NP) has emerged as a new two-dimensional material with improved stability compared to α -P, while it preserves the appealing electronic and mechanical properties of α -P. However, the phonon transport properties of α -NP remain poorly understood. In this study, we systematically compare phonon transport and thermal conductivity of α -NP and α -P by means of an iterative solution for the Boltzmann transport equation and first-principles calculations. We pay particular attention to careful enforcement of the Born-Huang sum rules on the interatomic force constants so that the flexural phonon branch of α -NP becomes perfectly quadratic close to the center of the Brillouin zone. We find that α -NP has a less anisotropic thermal conductivity compared to α -P, with the room-temperature values of 37.65 and 18.66 W m⁻¹ K⁻¹ in the armchair and zigzag directions, respectively. Interestingly, the anisotropy in the thermal conductivity of α -NP is found to be reversed compared to that of α -P, which has a higher thermal conductivity in the zigzag direction than the armchair direction. We found that as opposed to the usual understanding, considering only the directional dependence of the phonon group velocity fails to explain this reversed anisotropic thermal conductivity, and other phonon behaviors, such as avoided crossing of the acoustic and optical phonon branches, play a key role in determining the phonon relaxation time and thermal conductivity in α -NP. Our results may provide theoretical guidance for future fundamental studies on the anisotropic phonon thermal transport in low-dimensional materials, and they may also enable efficient heat management of nanoelectronic devices based on α -NP.

DOI: [10.1103/PhysRevMaterials.5.034009](https://doi.org/10.1103/PhysRevMaterials.5.034009)

I. INTRODUCTION

Since 2014, two-dimensional (2D) materials consisting of group V^A elements, namely phosphorene (P), arsenene (As), antimonene (Sb), and bismuthene (Bi), have become the focus of extensive research activities [1–5]. Single-layer phosphorene was the first developed member of this family possessing a variety of stable allotropes including puckered (known as α -P or black phosphorene) and buckled (known as β -P or blue phosphorene) honeycomb structures [1]. As opposed to many new 2D monolayers that are still in the theoretical study stage and have not yet been synthesized, single-layer black and blue phosphorene have been successfully fabricated using mechanical cleavage and liquid-phase exfoliation [6,7]. Interestingly, black phosphorene shows strong anisotropy in its electrical [8], mechanical [9,10], and thermal properties [11–13], which stems from its unique topological structure. In contrast to the semimetallic nature of graphene with a zero band gap, α -P is a semiconductor with a direct band gap of about ~ 1.5 eV which can be further modulated by layer thickness, functionalization, and in-plane strain. In addition, α -P possesses a carrier mobility of over 1000 cm² V⁻¹ s⁻¹ [1,6], higher than many other 2D materials such as MoS₂ (less than ~ 200 cm² V⁻¹ s⁻¹ [14]). From the thermal transport point of view, the thermal conductivity of α -P is known to be highly anisotropic [11–13], as its value along the zigzag (ZZ) direction is about 3.0 times higher than that

along the armchair (AM) direction [11]. The main reason for anisotropic thermal transport in α -P is attributed to the anisotropic behavior of phonon dispersion and group velocities along the zigzag and armchair directions. Despite these fascinating properties, practical applications of black phosphorene is seriously jeopardized by its poor stability under ambient conditions. Due to sp^3 hybridization, each phosphorus atom in α -P has two uncoupled electrons, which can lead to oxidation by oxygen and results in chemical degradation [15–17].

Very recently, monolayer nitrophosphorene (NP) as a 2D material belonging to group V^A-nitride (V^A-N) binary compounds has attracted considerable attention [17–20]. The larger cohesive energy of monolayer NP compared to that of phosphorene shows that the bonding in NP is stronger than that in phosphorene, an indication of enhanced air stability of monolayer NP [17,18]. Similar to phosphorene, previous studies have shown that nitrophosphorene also has different stable allotropes, namely α -, β -, and γ -phase [19,20]. Based on an energetic stability analysis by Xiao *et al.* [20], monolayer α -NP has the minimum formation energy between all group V^A-N binary compounds. This low formation energy substantially increases the chance of its experimental realization on proper substrates. For example, Ma *et al.* [19] proposed a possible growth method for α -NP on an Ag(110) substrate using the CVD method with cyclic phosphazenes. Also, a highly feasible strategy to prepare α -NP from its bulk counterpart by mechanical cleavage is proposed by Chen *et al.* [17]. Theoretical simulations have shown that monolayer

^{*}Corresponding author: chandraveer.singh@utoronto.ca

α -NP is a semiconductor with an indirect electronic band gap of 2.71 eV [17]. More importantly, the band gap is tunable via strain engineering or multilayer stacking [17,19]. Also, monolayer α -NP has a highly anisotropic electron mobility along the x and y directions. Its electron mobility along the x direction is as high as $\sim 4.9 \times 10^3 \text{ cm}^2 \text{ V}^{-1} \text{ s}^{-1}$, more than ten times higher than that along the y direction [17]. Interestingly, depending on the number of layers, few-layer α -NP sheets also possess a very high optical absorption coefficient that can reach the order of $\times 10^5 \text{ cm}^{-1}$ [17]. These outstanding electron mobility and adsorption coefficients make α -NP very promising as an efficient material to be used in photovoltaic solar cells. In particular, MoTe_2 /trilayer α -NP heterostructure is revealed to have a conversion efficiency up to about 16% [17]. From a mechanical point of view, it has been shown that α -NP is among those rare materials with a negative Poisson's ratio (NPR) [20]. Compared to conventional materials, materials with NPR have enhanced toughness, shear resistance, and vibration absorption. These properties make them very appealing for applications in medicine, tougher composites, and fasteners.

To put any of these fascinating potential applications into practice, a fundamental knowledge of the thermal transport properties in monolayer α -NP is key. To design efficient thermal, electronic, and optoelectronic devices based on α -NP, it is of vital technological importance to know whether it is among low or high thermal conductivity materials, how anisotropic is its thermal conductivity, and how do its phonon transport properties compare to other 2D materials. Investigation of the phonon thermal transport properties of α -NP has been known to be particularly challenging due to the difficulties in obtaining a physically correct phonon-dispersion curve from first-principles calculations. The flexural phonon branch (ZA mode) of α -NP presented in previous studies [17,19,21] shows either a small negative frequency pocket or linear components close to the center of the Brillouin zone (BZ). The presence of a linear or imaginary ZA branch in 2D materials can be caused by residual tensile or compressive strain in the system [22], and it can hinder an accurate prediction of the phonon thermal properties of unstrained freestanding 2D materials. Herein, a robust phonon transport analysis based on the Boltzmann transport equation (BTE) using *ab initio* calculations has been applied to compare the phonon transport properties of monolayer α -NP, including thermal conductivity, dispersion curve, group velocity, phase space, Grüneisen parameter, and relaxation time, to those of monolayer α -P. In our calculations, we use a postprocessing approach to carefully enforce the Born-Huang invariance conditions to obtain physically correct phonon dispersion, a very essential step toward a phonon thermal transport prediction of unstrained 2D materials. This correction ensures that the flexural phonon branch in an unstrained mono- or few-layer 2D material at the long-wavelength limit is perfectly quadratic, a long-lasting debate that has been proven by a very recent theoretical study [23]. It is known that this correction can have a significant effect on the predicted thermal conductivity of a 2D material, even to the point of reversing its anisotropy [24]. For example, in the case of borophene, the thermal conductivity predicted by corrected interatomic force constants (IFCs) is about 50% less than that predicted by unphysical uncorrected IFCs [24].

Our comparative study shows that α -NP has a reversed anisotropic thermal conductivity compared to that of phosphorene. Based on our result, the thermal conductivity of α -NP in the zigzag direction is much lower than that of α -P, but its thermal conductivity along the armchair direction is higher than the thermal conductivity of α -P in the same direction. Also, we found that in contrast with the usual assumption, only considering the directional dependence of phonon group velocity cannot explain the anisotropic phonon thermal transport in α -NP, and other phonon behaviors such as ‘‘avoided-crossing’’ can play an important role in determining the phonon lifetime and thermal conductivity.

II. COMPUTATIONAL METHODS

The computational workflow in this study starts with the geometry relaxation of α -NP and α -P. The four-atom unit cells of α -NP and α -P are fully relaxed by the QUANTUM ESPRESSO (QE) package [26] to obtain the optimized lattice constants and the atomic positions. A $30 \times 30 \times 1$ Monkhorst-Pack [27] \mathbf{k} -point mesh centered at the Γ -point is used to integrate the Brillouin zone (BZ). We use a Perdew-Burke-Ernzerhof (PBE) exchange-correlation functional with a projected augmented wave (PAW) pseudopotential, and electronic wave functions are expanded with plane waves up to an energy cutoff of 110 Ry. The energy and force convergence thresholds are set to 10^{-11} and 10^{-10} a.u., respectively. We also use a vacuum spacing of 20 Å along the z axis to eliminate the artificial interactions between adjacent layers. Figure 1 shows the optimized unit cell and a $3 \times 3 \times 1$ supercell of α -NP with the space group $Pmn21$ and α -P with the space group $Pmna$. The obtained optimized lattice constants (a and b) and the puckering distance (Δ) for α -NP and α -P are summarized in Table I. Our results are found to be in good agreement with previously reported values [17,20,28].

After obtaining the relaxed unit cell, the phonon calculations are carried out using the PHONOPY package [29] with a $10 \times 10 \times 1$ supercell to obtain the second-order IFCs. The raw second-order IFCs obtained directly from PHONOPY are then corrected using the HIPHIVE package [30] to ensure that they satisfy the Born-Huang invariance rules [24,30,31]. Next, the third-order anharmonic IFCs are calculated using a finite-difference method as implemented in the Thirdorder.py script [32] using slightly displaced $5 \times 5 \times 1$ supercells, with atomic interactions considered up to the 10th nearest neighbor. Having the set of second- and third-order IFCs, the lattice thermal conductivity along the α direction is computed on a well-converged $200 \times 200 \times 1$ \mathbf{q} -point mesh (see Figs. S1 and S2 in the supplemental material [33]) using the iterative approach to solve the BTE as implemented in the SHENGBTE code [32] as

$$\kappa_l^{\alpha\alpha} = \frac{1}{k_B T^2 \Omega N} \sum_{\lambda(\mathbf{q}, p)} n_\lambda^0 (1 + n_\lambda^0) (\hbar \omega_\lambda)^2 v_\lambda^\alpha F_\lambda^\alpha, \quad (1)$$

where T is the temperature, Ω is the unit-cell volume, N is the number of \mathbf{q} -point meshes used for the first BZ integration, $\lambda(\mathbf{q}, p)$ denotes a phonon mode with wave vector \mathbf{q} and polarization branch number p , n_λ^0 is the phonon occupation number based on the Bose-Einstein statistics, ω denotes

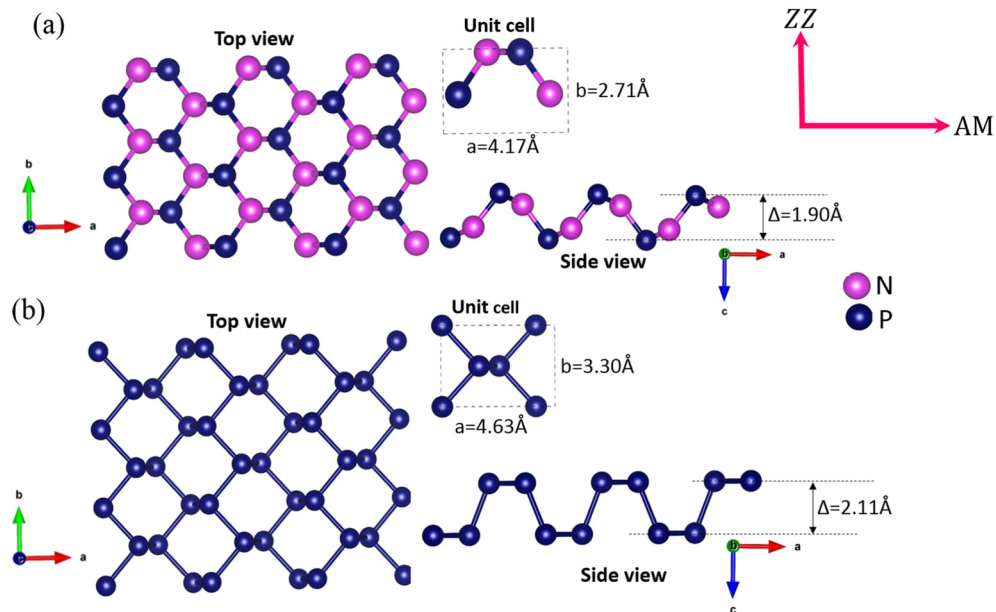


FIG. 1. The unit cell, and the top and side views of a $3 \times 3 \times 1$ supercell of (a) α -NP and (b) α -P. The lattice constants are shown by a and b , and the puckering height is denoted by Δ . The armchair and zigzag directions are also shown.

phonon frequency, v_λ^α represents the phonon group velocity in the direction α , and F_λ^α is given by

$$\mathbf{F}_\lambda = \tau_\lambda^0 (\mathbf{v}_\lambda + \mathbf{\Delta}_\lambda), \quad (2)$$

where τ_λ^0 is the relaxation time of mode λ as obtained from perturbation theory, and $\mathbf{\Delta}_\lambda$ is a correction term. More details about this method can be found in Ref. [32]. As can be seen in Eq. (1), the thermal conductivity of a system depends on its volume, which in turn depends on the thickness of the system. However, considering a thickness for 2D materials is challenging as it is not well-defined [34]. In this work, the thickness is chosen as the bulk interlayer spacing, which is $t = 6.35 \text{ \AA}$ for α -NP [19,35] and $t = 5.24 \text{ \AA}$ for α -P [35,36].

III. RESULTS AND DISCUSSION

The calculated phonon dispersion curve of α -NP and α -P can be seen in Figs. 2(a) and 2(c), respectively. As the unit cells of both monolayers have four atoms, there are a total of 12 phonon branches in their dispersion curves, three of which are acoustic modes including the out-of-plane flexural acoustic (ZA), the in-plane transversal acoustic (TA), and the in-plane longitudinal acoustic (LA), and the rest are optical modes.

TABLE I. The calculated lattice constants (a and b) and puckering distance (Δ) in α -NP and α -P monolayers.

Material	Reference	a (Å)	b (Å)	Δ (Å)
α -NP	This work	4.17	2.71	1.90
α -P	This work	4.63	3.30	2.11
α -NP	Ref. [20]	4.159	2.702	1.899
α -P	Ref. [25]	4.55	3.31	2.12

In Fig. 2(a), for α -NP monolayer we present both dispersion curves obtained by using the uncorrected (red dashed line) and corrected (blue line) second-order IFCs. Figure 2(b) also shows the zoomed dispersion curve of α -NP for frequencies lower than about 2.0 THz along the Γ -X direction. Based on Fig. 2(b), using the uncorrected IFCs to calculate the dispersion curve results in a small pocket of a “U”-shaped imaginary frequency region for the ZA phonon branch close to the Γ -point. This is a well-known unphysical artifact when one deals with the dispersion curve of 2D materials, and it is attributed to a breakdown of the continuous rotation symmetry caused by numerical inaccuracies, small residual stress in the system, the size of the supercell, the choice of cutoff values, and other settings adopted in the DFT calculation [37,38]. Although the presence of these small negative frequencies is not usually considered as a sign of kinetic instability of the system, it must be addressed before proceeding with any further phonon thermal transport analysis [24]. In this study, we correct the “raw” (uncorrected) IFCs obtained from DFT using a robust postprocessing approach by enforcing the Born-Huang invariance rules. In this approach, the Born-Huang sum rule is expressed as a constrained optimization problem that can be solved by, for example, ridge regression using the l_2 -norm. The details of the mathematical formalism of this approach can be found in Ref. [30]. After postprocessing of the “raw” IFCs, we recalculate the dispersion curve with the “corrected” second-order IFCs [blue curves in Figs. 2(a) and 2(b)]. Here we emphasize that (i) by using the corrected second-order IFC, not only does the negative frequency region completely disappear, but also the ZA mode branch close to the Γ -point becomes completely quadratic, which is a necessary condition in few-layer 2D materials based on the thin-film elastic theory [23,24]; and (ii) the change in other phonon branches including TA, LA, and optical modes after imposing the correction is very small. These phonon modes in the corrected dispersion are almost indistinguishable

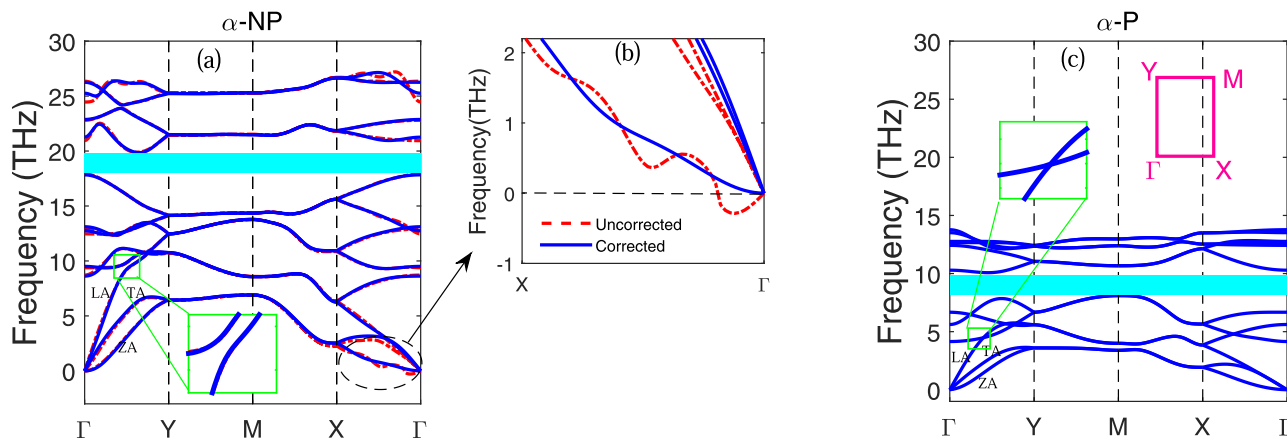


FIG. 2. (a) Phonon dispersion curve of α -NP using both uncorrected and corrected second-order IFCs, (b) zoomed phonon dispersion of α -NP along the Γ -X direction, and (c) phonon dispersion curve of α -P. The insets in (a) and (c) show the enlargements of the green squares.

from the same modes in the uncorrected dispersion to the naked eye.

We note that the dispersion curves of both α -NP and α -P are in good agreement with recent studies [11,17,19], except for the fact that our predicted ZA phonon branch for α -NP near the Γ -point in all directions is perfectly quadratic, while obvious unphysical linear components, particularly along the Γ -Y path, can be seen in previous works [17,19]. Now we compare the corrected dispersion curve of α -NP with that of α -P. Based on Figs. 2(a) and 2(c), α -NP generally has higher phonon frequencies than α -P, which can be attributed to the stronger atomic bond of N-P compared to P-P, and also the lighter atomic mass of nitrogen compared to that of phosphorus. The highest optical frequency in α -NP is about 27.0 THz, almost two times higher than that of α -P, which is about 13.7 THz. The phonon gaps in both monolayers are shown as highlighted areas in Figs. 2(a) and 2(c). We found that two monolayers have very similar phonon gaps, which are about 2.02 and 1.98 THz for α -NP and α -P, respectively. Moreover, it can be seen that both monolayers exhibit an anisotropic phonon-dispersion curve along the Γ -Y (zigzag) and Γ -X (armchair) directions, which originated from their puckered hingelike structure. As an example of this behavior, the LA phonon branch of both monolayers has a larger slope along the Γ -Y direction than that along the Γ -X direction. This can lead to an orientation dependence of the group velocity, stiffness, elastic constants, and the thermal conductivity in these systems, which will be discussed in detail later.

Now, we discuss a striking difference between the dispersion curves of these two monolayers. As can be seen in the insets of Figs. 2(a) and 2(c), the “avoided crossing” between the LA mode and the low optical modes can be clearly seen along the Γ -Y direction in α -NP, but not in α -P. Avoided crossing is an indication of strong coupling (hybridization) between the acoustics and optic modes. This different behavior observed in α -NP and α -P can be attributed to their different symmetry and level of anharmonic repulsion between acoustic modes and low-lying optical modes. It is known that the avoided crossing can lead to shorter phonon lifetimes and lower thermal conductivity [39–41].

The calculated lattice thermal conductivity of α -NP and α -P along the armchair (AM) and zigzag (ZZ) directions

obtained from the iterative solution of the BTE as a function of temperature (T) ranging from 200 to 800 K can be seen in Fig. 3 (see Fig. S3 in the supplemental material [33] for a comparison between the iterative solution and the RTA). In our thermal conductivity calculation, we use thicknesses of 6.35 and 5.24 Å for α -NP and α -P, respectively. It can be seen that all the thermal conductivity values almost have a T^{-1} dependence, which confirms that for both monolayers the umklapp anharmonic three-phonon process plays a dominant role in the phonon thermal transport within the considered temperature range. The calculated thermal conductivity of α -P at 300 K is strongly anisotropic as its value along the ZZ direction, $\kappa_{ZZ} = 108.0 \text{ W m}^{-1} \text{ K}^{-1}$, is almost five times higher than that along the AM direction, $\kappa_{AM} = 22.0 \text{ W m}^{-1} \text{ K}^{-1}$. These values are in good agreement with previous studies [11,12,28], which confirms the reliability of our computational approach here. Very interestingly, we find that κ in α -NP is less anisotropic in comparison with α -P and α -As [42], but its anisotropy is reversed compared to these monolayers as its thermal conductivity along the AM direction is almost two times higher

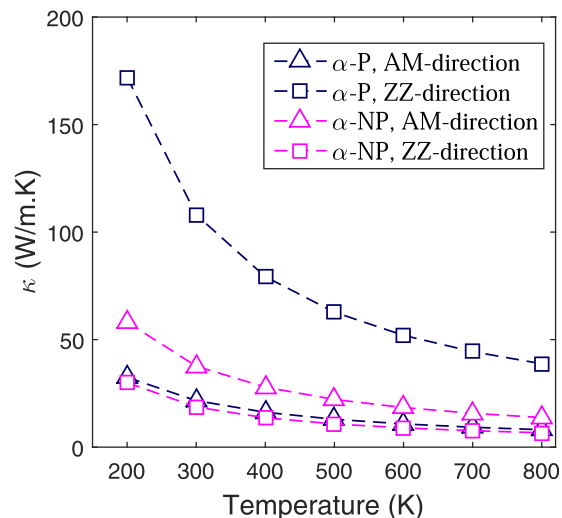


FIG. 3. Calculated lattice thermal conductivity of α -NP and α -P along the armchair and zigzag directions as a function of temperature.

TABLE II. Predicted room-temperature (300 K) thermal conductivity of α -NP and α -P as well as some other 2D materials along the zigzag and armchair directions. The methodology used in each study is based on the iterative solution of the BTE combined with DFT calculations. The thickness value adopted in each study is also presented.

Material	Reference	Thickness (\AA)	k_{ZZ} ($\text{W m}^{-1} \text{K}^{-1}$)	k_{AM} ($\text{W m}^{-1} \text{K}^{-1}$)
α -NP	This work	6.35	18.66	37.65
α -P	This work	5.24	108.0	22.0
α -As	Zeraati <i>et al.</i> [42]		30.4	7.8
α -Sb	Zheng <i>et al.</i> [28]	6.16	8.4	4.1
α -PO	Lee <i>et al.</i> [47]	8.0	7.08	2.42
Silicene	Peng <i>et al.</i> [46]	4.20	28.3	28.3
Graphene	Kuang <i>et al.</i> [43]	3.35	5450	5450
C_3N	Taheri <i>et al.</i> [45]	3.20	348	348
Stanene	Peng <i>et al.</i> [46]	4.34	5.8	5.8
Germanene	Peng <i>et al.</i> [46]	4.22	2.4	2.4

than that along the ZZ direction. Based on our results, the predicted κ value of α -NP in the AM direction is $\kappa_{AM} = 37.65 \text{ W m}^{-1} \text{K}^{-1}$ while it is $\kappa_{ZZ} = 18.66 \text{ W m}^{-1} \text{K}^{-1}$ along the ZZ direction. This unique anisotropy can make α -NP a highly promising candidate to be used in devices for which due to thermal and design constraints the AM direction needs to be thermally more conductive than the ZZ direction. Compared to α -P, monolayer α -NP has about 5.7 times lower thermal conductivity along the ZZ direction; however, its thermal conductivity along the AM direction is almost 1.7 times higher than that of α -P. As high thermal conductivity is important for thermal management applications, and low thermal conductivity, on the other hand, is an imperative feature of a high-performance thermoelectric material, α -NP can be a potential alternative for α -P in a wide range of applications. We also compare the room-temperature κ value of α -NP with some other 2D materials in Table II. As can be seen, α -NP has much lower thermal conductivity than graphene [43,44] and C_3N [45]. However, its thermal conductivity is higher than or comparable to silicene [46], phosphorene oxide (PO) [47], puckered arsenene (α -As) [28], puckered antimonene (α -Sb) [28], buckled stanene [46], and buckled germanene [46].

Next, we focus on the contribution of each phonon mode to the total lattice thermal conductivity of α -NP and α -P at room temperature. Table III summarizes the contribution of different phonon branches to the thermal conductivity for α -NP and α -P along the AM and ZZ directions. First, we emphasize

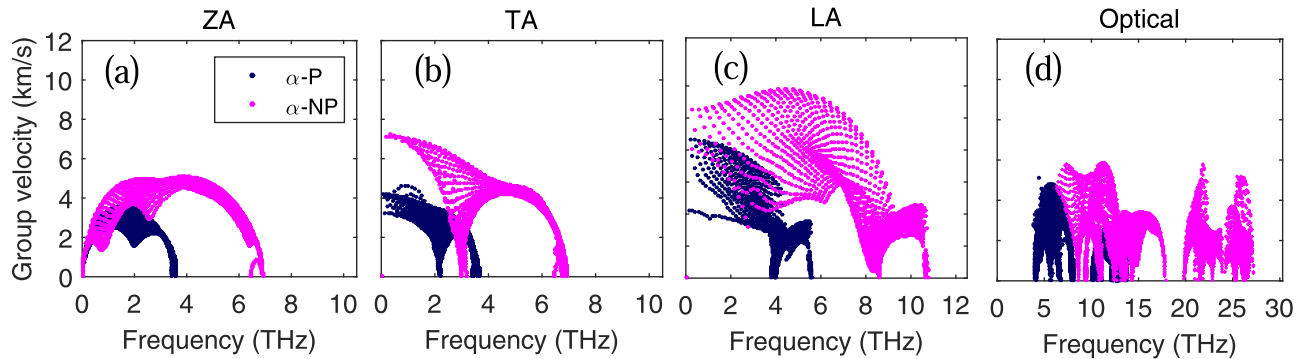
TABLE III. Percentage contribution (%) of different phonon modes to the thermal conductivity of α -NP and α -P at 300 K along the armchair and zigzag directions.

	α -NP	α -P
ZA-AM	1.0	8.0
ZA-ZZ	29.5	34.0
TA-AM	86.5	13.0
TA-ZZ	22.0	23.5
LA-AM	9.0	34.0
LA-ZZ	41.0	30.0
Optical-AM	3.5	45.0
Optical-ZZ	7.5	12.5

that our predicted contributions of different modes for α -P are in good agreement with previous studies [11,12]. Based on Table III, the ZA mode in α -NP has a very low contribution of about 1% to the thermal conductivity along the AM direction; however, its contribution increases to a value of 29.5% along the ZZ direction. We note that these values are much lower than the contribution of the ZA branch to the thermal conductivity of graphene, which is known to be about 80% [43], and silicene (about 67.3% [46]). Stemming from the flat structure of graphene, the ZA mode has mirror symmetry, which only allows phonon-phonon scattering processes involving an even number of ZA phonons [48]. For example, a process such as $\text{ZA} + \text{TA} \rightarrow \text{LA}$ is forbidden in graphene as it has an odd number of ZA phonons involved. This makes the lifetime of the ZA branch much longer than that of the TA and LA modes, leading to the high contribution of this mode. In α -NP and α -P, however, the atomic structure is puckered (not flat) and the mirror symmetry does not exist, so the contribution from the ZA mode to the κ value is much lower than that in graphene.

Based on Table III, the TA (LA) mode is the dominant mode in thermal transport of α -NP in the AM (ZZ) direction, responsible for about 86.5% (41%) of the thermal conductivity in this direction. Moreover, we note that the contribution from the optical phonons in the κ value of α -P is higher than that in α -NP and many other 2D materials [46], particularly in the AM direction. This may be caused by the relatively high group velocity of optical phonons in α -P, and also the overlap between the LA mode and low-frequency optical modes [Fig. 2(c)]. Next, we examine different key phonon properties such as group velocity and lifetime to better understand the roots of the differences in phonon thermal transport of α -NP and α -P.

The group velocities of different phonon modes defined as $\mathbf{v}_g = \frac{d\omega}{d\mathbf{q}}$ in α -NP and α -P are plotted in Fig. 4. First, we note that the group velocity of the ZA mode for both monolayers close to the Γ -point vanishes. In other words, for the ZA branch we have $\lim_{\mathbf{q} \rightarrow 0} \frac{d\omega}{d\mathbf{q}} = 0$. This confirms that the ZA branch is perfectly quadratic close to the Γ -point, a must for any phonon thermal transport analysis based on the BTE in 2D materials [23,24]. As can be seen in Figs. 4(a)–4(d), for most of the phonon modes α -NP has generally higher group velocity than α -P, which is expected due to the higher phonon frequencies in its dispersion curve (Fig. 2). The


 FIG. 4. Phonon group velocity of (a) ZA, (b) TA, (c) LA, and (d) optical modes in α -NP and α -P.

highest group velocities of the ZA, TA, LA, and optical modes in α -NP (α -P) are 5.0 (3.5), 7.0 (4.6), 11.7 (8.6), and 5.8 (4.8) km/s, respectively. Thus, group velocity can partly explain the higher thermal conductivity of α -NP than α -P along the AM direction (Fig. 3). However, it fails to explain the much higher κ value of α -P compared to α -NP in the ZZ direction, and other contributing factors must be considered.

To shed light on the anisotropic thermal transport in these monolayers, the Γ -point group velocities of the LA and TA modes along the AM and ZZ directions are listed in Table IV. The predicted group velocities of α -P are in excellent agreement with previously reported values [12,49]. As can be seen, the group velocity of the LA mode in both α -NP and α -P is anisotropic, while the TA mode has almost an isotropic group velocity. In both systems, the group velocity of the LA mode has a higher value along the ZZ direction compared to that along the AM direction. The ratio of the Γ -point LA group velocity in the ZZ direction to that along the AM direction is about 1.3 in α -NP and 2.0 in α -P, which shows that α -NP is less anisotropic than α -P.

Based on Fig. 3, we found that $\kappa_{\alpha-P}^{ZZ} > \kappa_{\alpha-P}^{AM}$ and $\kappa_{\alpha-NP}^{AM} > \kappa_{\alpha-NP}^{ZZ}$. Although the former can be well explained by the higher group velocity of the LA mode in the ZZ direction than that along the AM direction, group velocity by its own fails to explain why α -NP has a higher thermal conductivity in the AM direction than the ZZ direction. In other words, the anisotropy predicted by the group velocity in α -NP is exactly opposite to the actual trend observed for thermal conductivity (Fig. 3). Our finding highlights the fact that considering only the orientation-dependent group velocity is not sufficient to understand the anisotropic thermal transport in 2D materials.

To better understand the differences in the thermal conductivity of α -NP and α -P, we next study the phonon lifetime

as one of the most important parameters contributing to the thermal conductivity of a system [see Eqs. (1) and (2)]. The mode-by-mode lifetimes of α -NP and α -P are plotted in Fig. 5. As can be seen in Fig. 5(a), for most of the ZA phonons, α -P has a much longer lifetime than α -NP. The difference for some ZA modes is even more than one order of magnitude. Regarding the TA mode [Fig. 5(b)], the difference between the phonon lifetime of α -NP and α -P is not as high as the ZA mode. Also, based on Figs. 5(c) and 5(d), it can be seen that the LA and optical modes have longer lifetimes in α -P than α -NP. The fact that the phonon lifetime of most of the phonon branches in α -P is longer than those in α -NP can explain the much higher κ value of α -P along the ZZ direction than α -NP, despite its lower group velocity (see Figs. 3 and 4).

As we discussed before, the reversed anisotropic thermal conductivity of α -NP compared to α -P is one of our interesting findings in this study. Now we elucidate the reason behind this behavior using directional phonon lifetimes. Figures S4(a) and S4(b) in the supplemental material [33] show the phonon lifetime of all the acoustic modes (ZA, LA, and TA) in α -NP and α -P along the ZZ and AM directions. Based on Fig. S4(a), the acoustic modes of α -P along the ZZ direction have a longer lifetime than those along the AM direction, in agreement with previous findings [49]. The longer phonon lifetime of acoustic modes along the ZZ direction together with the higher group velocity of the LA mode along the same direction are the reasons for the higher κ value of α -P along the ZZ direction than that along the AM direction. However, the situation is reversed in α -NP. Based on Fig. S4(b), some acoustic modes along the AM direction have a much longer lifetime than the ZZ direction. Based on our result, the longer lifetime of acoustic modes along the AM direction can more than compensate for the slightly higher group velocity of the LA mode along the ZZ direction, resulting in higher thermal conductivity in the AM direction. To better clarify this, for both monolayers we also plotted the directional lifetime of only the LA mode, the mode with the anisotropic group velocity, in Figs. S4(c) and S4(d). It can clearly be seen that in α -P, the LA mode has a longer lifetime along the ZZ direction. However, for α -NP the LA mode lifetime along the AM direction is longer. This behavior can be attributed to the ‘‘avoid-crossing’’ of the LA mode, and the low-lying optical branches occurring along the ZZ (Γ -Y) direction in α -NP [Fig. 2(a)].

 TABLE IV. Group velocity (in km/s) of the LA and TA modes along the zigzag and armchair directions at the Γ -point in α -NP and α -P monolayers.

	α -NP	α -P
LA-ZZ	10.5	8.6
LA-AM	8.1	4.2
TA-ZZ	7.1	4.2
TA-AM	7.1	4.1

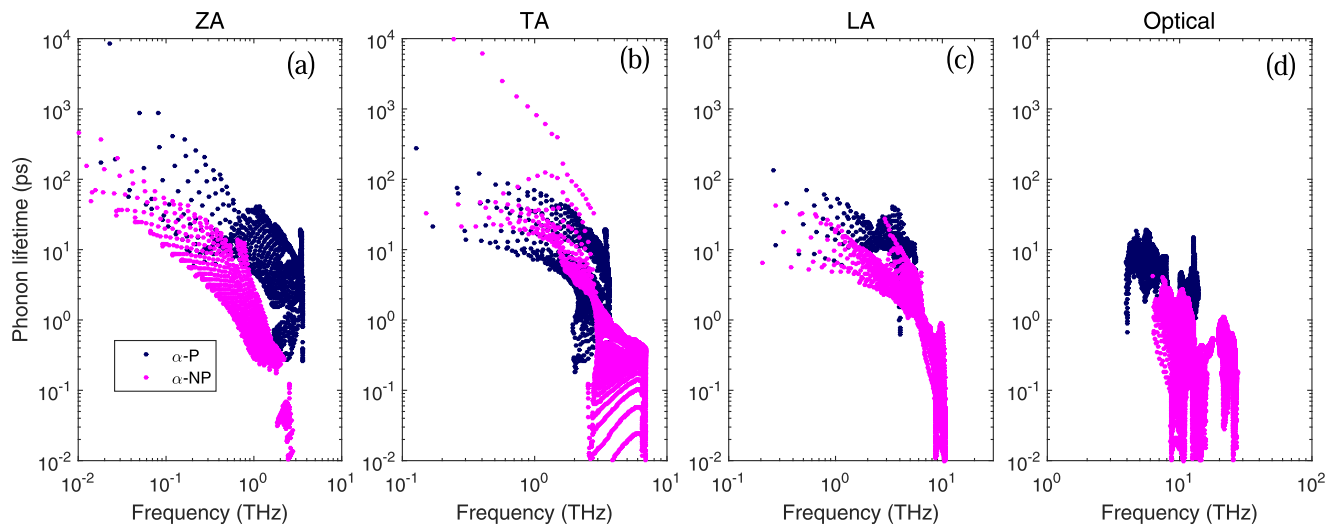


FIG. 5. Phonon lifetime of (a) ZA, (b) TA, (c) LA, and (d) optical modes in α -NP and α -P.

The phonon lifetime of a system is generally determined by two parameters: (i) the number of available three-phonon scattering channels that satisfy the conservation of energy and momentum rules, and (ii) the strength of these channels. The first one can be measured by the so-called “weighted phase space (W)” defined as [50,51]

$$W_{\lambda}^{\pm} = \frac{1}{2N} \sum_{\lambda'p'} \left\{ \begin{array}{l} 2(n'_{\lambda} - n''_{\lambda}) \\ n'_{\lambda} + n''_{\lambda} + 1 \end{array} \right\} \frac{\delta(\omega_{\lambda} \pm \omega_{\lambda'} - \omega_{\lambda''})}{\omega_{\lambda} \omega_{\lambda'} \omega_{\lambda''}}. \quad (3)$$

Generally, a higher value of W indicates that there are more available scattering channels for phonons, which results in a shorter lifetime and lower thermal conductivity. Figure 6 compares the value of W in α -P and α -NP for each phonon mode. As can be seen, for all the phonon modes α -NP has a higher W , which explains the shorter lifetime of α -NP compared to α -P.

The strength of the available three-phonon scattering channels is also important in determining the lifetime and

the thermal conductivity in a crystal. The mode-dependent Grüneisen parameter (γ_{λ}) is usually used as a measure of the anharmonicity of a system, determining the strength of three-phonon scattering processes. This parameter is related to the third-order anharmonic IFCS as

$$\gamma_{\lambda} = -\frac{1}{6\omega_{\lambda}^2} \sum_{ijk\alpha\beta\gamma} \frac{e_{i\alpha}^{\lambda*} e_{j\beta}^{\lambda}}{\sqrt{M_i M_j}} r_k^{\lambda} \Phi_{ijk}^{\alpha\beta\gamma} \exp(i\mathbf{q} \cdot \mathbf{r}_j), \quad (4)$$

where α , β , and γ are the Cartesian components; i , j , and k are the atomic indices; M_i represents the mass of the atom i ; $e_{i\alpha}^{\lambda}$ is the phonon eigenvector of atom i in the α direction; \mathbf{r}_i is the position vector of the i th atom, and $\Phi_{ijk}^{\alpha\beta\gamma}$ represents the third-order anharmonic IFCS. It is known that the Grüneisen parameter is inversely correlated with the phonon lifetime and the thermal conductivity of a system [52]. In Fig. 7 we compare the value of the Grüneisen parameters, $|\gamma_{\lambda}|$, for each phonon mode. As can be seen in Fig. 7(a), $|\gamma_{\lambda}|$ for the ZA mode in the low-frequency region close to the Γ -point has

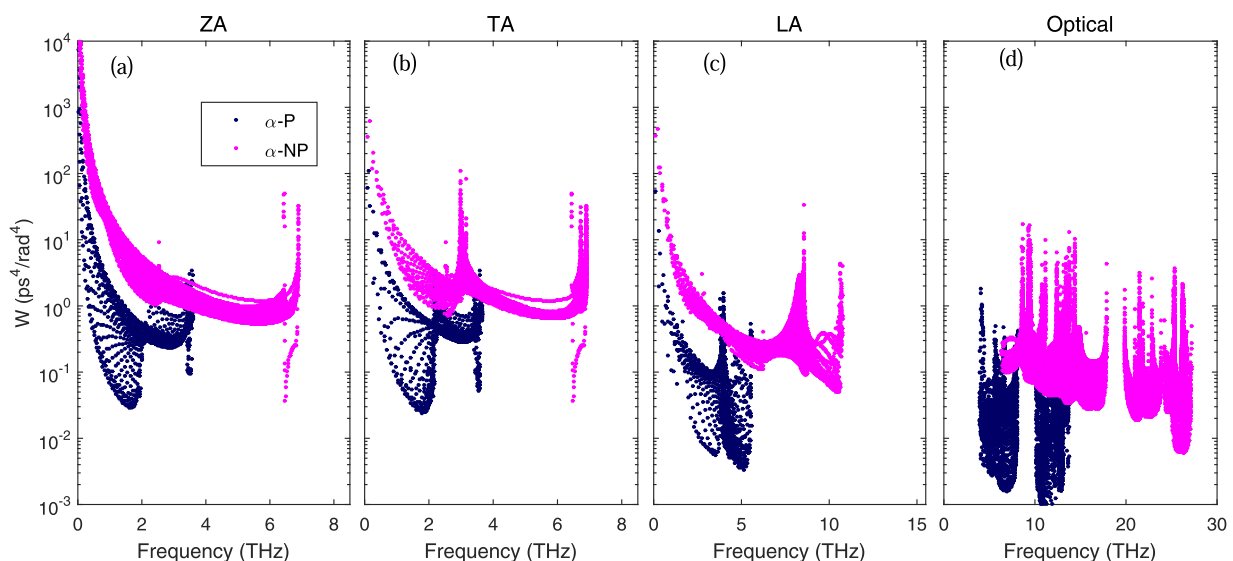


FIG. 6. Three-phonon phase space of (a) ZA, (b) TA, (c) LA, and (d) optical modes in α -NP and α -P.

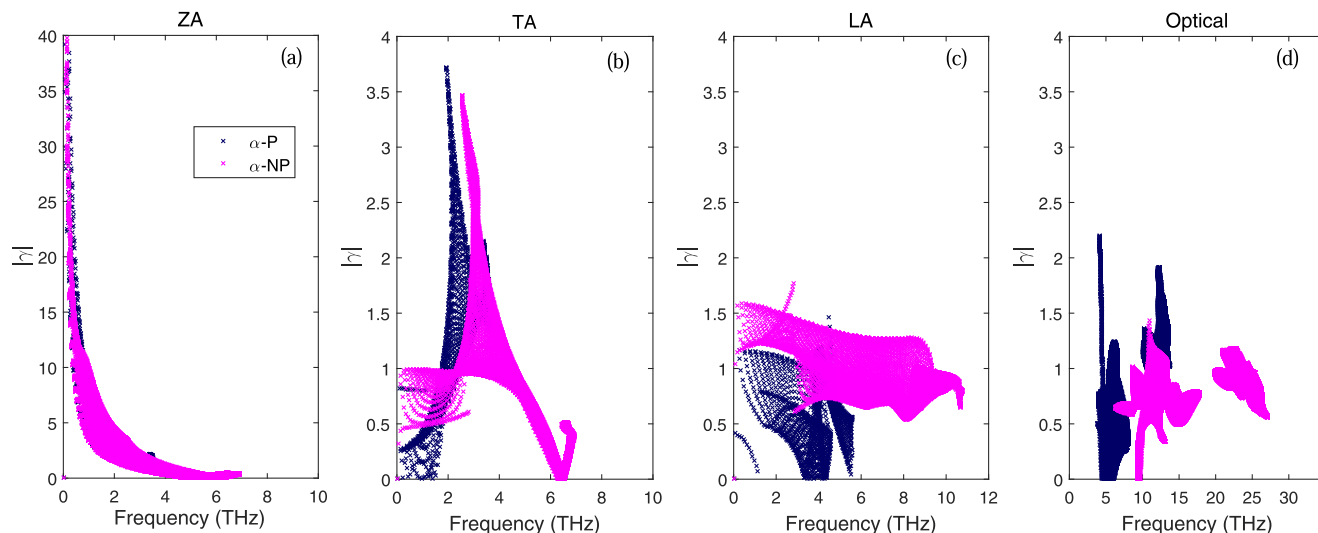


FIG. 7. Absolute value of the Grüneisen parameters of (a) ZA, (b) TA, (c) LA, and (d) optical modes in α -NP and α -P.

very large values in both monolayers, which is known as a signature of 2D materials [53].

Based on Figs. 7(a)–7(d), except for the LA mode, we do not find a significant difference between the $|\gamma_\lambda|$ value in these two systems. However, $|\gamma_\lambda|$ of the LA mode in α -NP is clearly higher than that in α -P, which is an indication of larger total anharmonicity in α -NP compared to α -P, in agreement with the shorter lifetime observed in α -NP.

One effective way to modulate the thermal conductivity of a system is by changing the grain size of the crystal. Usually, size reduction decreases the phonon mean free path (MFP) and results in a lower thermal conductivity while it does not change the electronic conductivity. This can greatly enhance the thermoelectric figure of merit in the system. Plotted in Fig. 8 is the normalized thermal conductivity accumulation as a function of MFP at 300 K for α -NP and α -P. To further evaluate which range of phonon MFP contributes more to the κ value, we calculated the phonon MFP in which the accumulated thermal conductivity is 50% of its ultimate value

[$\kappa(l_0)/\kappa_\infty = 1/2$]. Listed in Table V is our calculated value of l_0 . We confirm that our predicted values of l_0 for α -P agree well with previously reported values by Ref. [12]. Very interestingly, we found that the l_0 value for α -NP is also strongly anisotropic along the AM and ZZ directions. This means that by reducing the grain size of the system, thermal conductivity along the AM will be much more affected than that along the ZZ direction. Such high anisotropy in l_0 was also previously reported for γ -phase phosphorene (γ -P) [12], and it is known to be very appealing for design purposes as it offers extra flexibility to optimize the thermal conductivity along the AM direction.

IV. SUMMARY AND CONCLUSIONS

We present a comparative study on the phonon thermal transport of novel α -nitrophosphorene monolayer and α -phosphorene based on the Boltzmann transport equation and first-principles density functional theory calculations. We pay

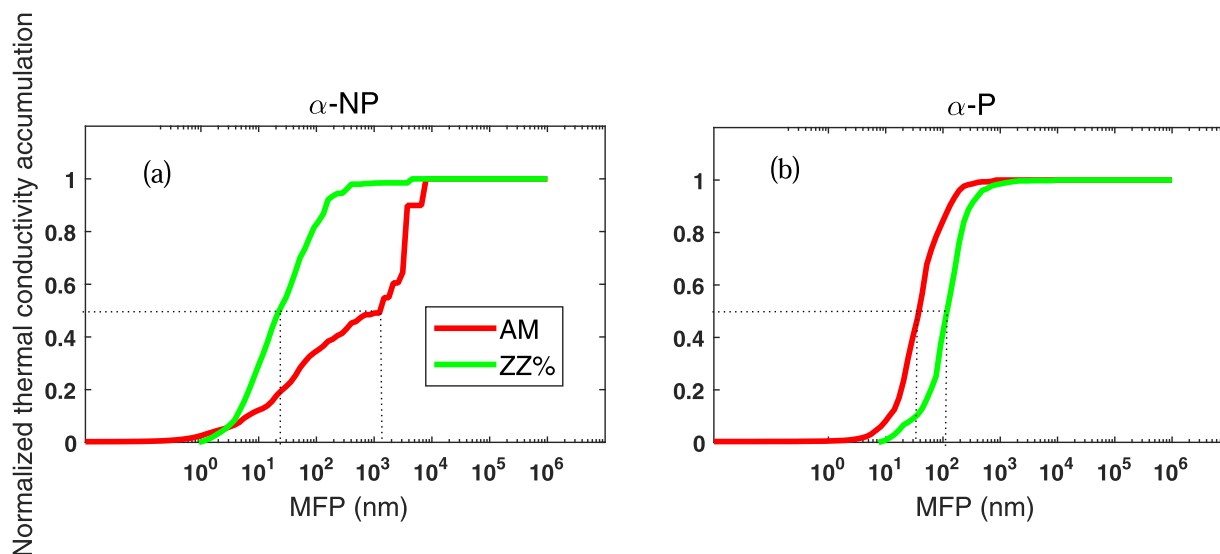


FIG. 8. The normalized thermal conductivity accumulation at room temperature as a function of phonon MFP for (a) α -NP and (b) α -P.

TABLE V. The MFP value (in nm) which corresponds to 50% of thermal conductivity accumulation for α -NP and α -P along the zigzag and armchair directions at 300 K.

	α -NP	α -P
ZZ	21	109
AM	1200	29

particular attention to enforcement of the Born-Huang sum rules on the second-order interatomic force constants obtained from density functional theory using a postprocessing approach so that they become physically correct.

We find that the thermal conductivity of α -NP along the armchair direction, $\kappa_{AM} = 37.65$, is about two times higher than that along the zigzag direction, $\kappa_{ZZ} = 18.66 \text{ W m}^{-1} \text{ K}^{-1}$. This level of anisotropy is less than what has been found for α -P, α -As, and many other 2D materials. However, we demonstrate that the anisotropy in α -NP is unique as it is opposite to α -P, which has a higher thermal conductivity along the zigzag direction than that along the armchair direction. Our analyses show that although the group velocity of the LA mode in α -NP is found to be higher along the zigzag direction than that along the armchair direction, a longer lifetime of acoustic phonons along the armchair direction can more than compensate for the effect of the group velocity. Based on the dispersion curve of α -NP, the shorter lifetime of the acoustic modes along the zigzag direction can be attributed to the observed “avoid-crossing” between the LA modes and the low optical modes. After comparing the thermal conductivity

of α -NP with α -P, we find that the thermal conductivity of α -NP along the zigzag direction is about six times lower than that of α -P, but its thermal conductivity along the armchair direction is about 1.7 times higher than that of α -P. Our results show that α -NP has generally higher phonon frequencies and group velocity than α -P, but it has shorter phonon lifetimes. The shorter phonon lifetime of α -NP is mainly attributed to its higher three-phonon scattering phase space, and also the higher Grüneisen parameter of the LA mode compared to those in α -P. Finally, we demonstrate that the thermal conductivity of α -NP, particularly in the armchair direction, is highly tunable by changing the size of the system. Our results can provide a helpful guideline not only for future fundamental studies on 2D materials and heterostructures, but also for efficient design of emerging thermoelectric and optoelectronics nanodevices based on novel low-dimensional materials.

The data that support the findings of this study are available from the corresponding author upon reasonable request.

ACKNOWLEDGMENTS

This work was supported by the Natural Sciences and Engineering Research Council of Canada (NSERC), University of Toronto. Computations were performed on the Niagara supercomputer at the SciNet HPC Consortium. SciNet is funded by the Canada Foundation for Innovation under the auspices of Compute Canada, the Government of Ontario, Ontario Research Fund Research Excellence, and the University of Toronto.

- [1] H. Liu, A. T. Neal, Z. Zhu, Z. Luo, X. Xu, D. Tománek, and P. D. Ye, Phosphorene: An unexplored 2d semiconductor with a high hole mobility, *ACS nano* **8**, 4033 (2014).
- [2] C. Kamal and M. Ezawa, Arsenene: Two-dimensional buckled and puckered honeycomb arsenic systems, *Phys. Rev. B* **91**, 085423 (2015).
- [3] S. Zhang, S. Guo, Z. Chen, Y. Wang, H. Gao, J. Gómez-Herrero, P. Ares, F. Zamora, Z. Zhu, and H. Zeng, Recent progress in 2d group-va semiconductors: from theory to experiment, *Chem. Soc. Rev.* **47**, 982 (2018).
- [4] S. Zhang, M. Xie, F. Li, Z. Yan, Y. Li, E. Kan, W. Liu, Z. Chen, and H. Zeng, Semiconducting group 15 monolayers: A broad range of band gaps and high carrier mobilities, *Angew. Chem.* **128**, 1698 (2016).
- [5] A. Taheri, C. Da Silva, and C. H. Amon, Effects of biaxial tensile strain on the first-principles-driven thermal conductivity of buckled arsenene and phosphorene, *Phys. Chem. Chem. Phys.* **20**, 27611 (2018).
- [6] L. Li, Y. Yu, Guo J. Ye, Q. Ge, X. Ou, H. Wu, D. Feng, Xian H. Chen, and Y. Zhang, Black phosphorus field-effect transistors, *Nat. Nanotechnol.* **9**, 372 (2014).
- [7] W. Lu, H. Nan, J. Hong, Y. Chen, C. Zhu, Z. Liang, X. Ma, Z. Ni, C. Jin, and Z. Zhang, Plasma-assisted fabrication of monolayer phosphorene and its raman characterization, *Nano Res.* **7**, 853 (2014).
- [8] R. Fei and L. Yang, Strain-engineering the anisotropic electrical conductance of few-layer black phosphorus, *Nano Lett.* **14**, 2884 (2014).
- [9] L. Wang, A. Kutana, X. Zou, and B. I. Yakobson, Electro-mechanical anisotropy of phosphorene, *Nanoscale* **7**, 9746 (2015).
- [10] Q. Wei and X. Peng, Superior mechanical flexibility of phosphorene and few-layer black phosphorus, *Appl. Phys. Lett.* **104**, 251915 (2014).
- [11] A. Jain and A. J. H. McGaughey, Strongly anisotropic in-plane thermal transport in single-layer black phosphorene, *Sci. Rep.* **5**, 8501 (2015).
- [12] J. Zhang, H. J. Liu, L. Cheng, J. Wei, J. H. Liang, D. D. Fan, P. H. Jiang, and J. Shi, Thermal conductivities of phosphorene allotropes from first-principles calculations: A comparative study, *Sci. Rep.* **7**, 4623 (2017).
- [13] G. Qin, Q.-B. Yan, Z. Qin, S.-Y. Yue, M. Hu, and G. Su, Anisotropic intrinsic lattice thermal conductivity of phosphorene from first principles, *Phys. Chem. Chem. Phys.* **17**, 4854 (2015).
- [14] S. Yu, H. D. Xiong, K. Eshun, H. Yuan, and Q. Li, Phase transition, effective mass and carrier mobility of mos2 monolayer under tensile strain, *Appl. Surf. Sci.* **325**, 27 (2015).
- [15] A. Favron, E. Gaufrès, F. Fossard, A.-L. Phaneuf-L'Heureux, N. Y. W. Tang, P. L. Lévesque, A. Loiseau, R. Leonelli, S. Francoeur, and R. Martel, Photooxidation and quantum

- confinement effects in exfoliated black phosphorus, *Nat. Mater.* **14**, 826 (2015).
- [16] M. Akhtar, G. Anderson, R. Zhao, A. Alruqi, J. E. Mroczkowska, G. Sumanasekera, and J. B. Jasinski, Recent advances in synthesis, properties, and applications of phosphorene, *npj 2D Mater. Appl.* **1**, 5 (2017).
- [17] Y. Chen, Z. Lao, B. Sun, X. Feng, S. A. T. Redfern, H. Liu, J. Lv, H. Wang, and Z. Chen, Identifying the ground-state np sheet through a global structure search in two-dimensional space and its promising high-efficiency photovoltaic properties, *ACS Mater. Lett.* **1**, 375 (2019).
- [18] L. Zhao, W. Yi, J. Botana, F. Gu, and M. Miao, Nitro-phosphorene: A 2d semiconductor with both large direct gap and superior mobility, *J. Phys. Chem. C* **121**, 28520 (2017).
- [19] S. Ma, C. He, L. Z. Sun, H. Lin, Y. Li, and K. W. Zhang, Stability of two-dimensional pn monolayer sheets and their electronic properties, *Phys. Chem. Chem. Phys.* **17**, 32009 (2015).
- [20] W.-Z. Xiao, G. Xiao, Q.-Y. Rong, and L.-L. Wang, Theoretical discovery of novel two-dimensional va-n binary compounds with auxiticity, *Phys. Chem. Chem. Phys.* **20**, 22027 (2018).
- [21] W. Yu, C.-Y. Niu, Z. Zhu, X. Wang, and W.-B. Zhang, Atomically thin binary v-v compound semiconductor: a first-principles study, *J. Mater. Chem. C* **4**, 6581 (2016).
- [22] R. Roldán, A. Fasolino, K. V. Zakharchenko, and M. I. Katsnelson, Suppression of anharmonicities in crystalline membranes by external strain, *Phys. Rev. B* **83**, 174104 (2011).
- [23] Y. Kuang, L. Lindsay, Q. Wang, and L. He, Lattice chain theories for dynamics of acoustic flexural phonons in nonpolar nanomaterials, *Phys. Rev. B* **102**, 144301 (2020).
- [24] J. Carrete, W. Li, L. Lindsay, D. A. Broido, L. J. Gallego, and N. Mingo, Physically founded phonon dispersions of few-layer materials and the case of borophene, *Mater. Res. Lett.* **4**, 204 (2016).
- [25] F. Ersan, E. Aktürk, and S. Ciraci, Stable single-layer structure of group-v elements, *Phys. Rev. B* **94**, 245417 (2016).
- [26] P. Giannozzi, S. Baroni, N. Bonini, M. Calandra, R. Car, C. Cavazzoni, D. Ceresoli, G. L. Chiarotti, M. Cococcioni, I. Dabo, *et al.*, Quantum espresso: a modular and open-source software project for quantum simulations of materials, *J. Phys.: Condens. Matter* **21**, 395502 (2009).
- [27] J. D. Pack and H. J. Monkhorst, special points for Brillouin-zone integrations a reply, *Phys. Rev. B* **16**, 1748 (1977).
- [28] G. Zheng, Y. Jia, S. Gao, and S.-H. Ke, Comparative study of thermal properties of group-va monolayers with buckled and puckered honeycomb structures, *Phys. Rev. B* **94**, 155448 (2016).
- [29] A. Togo, F. Oba, and I. Tanaka, First-principles calculations of the ferroelastic transition between rutile-type and cacl 2-type sio 2 at high pressures, *Phys. Rev. B* **78**, 134106 (2008).
- [30] F. Eriksson, E. Fransson, and P. Erhart, The hiphive package for the extraction of high-order force constants by machine learning, *Adv. Theory Simul.* **2**, 1800184 (2019).
- [31] M. Born and K. Huang, *Dynamical Theory of Crystal Lattices* (Oxford University Press, Oxford, 1954).
- [32] W. Li, J. Carrete, N. A. Katcho, and N. Mingo, Shengbte: A solver of the boltzmann transport equation for phonons, *Comput. Phys. Commun.* **185**, 1747 (2014).
- [33] Please see the supplemental material at <http://link.aps.org/supplemental/10.1103/PhysRevMaterials.5.034009> for convergence tests of thermal conductivity, comparison between the iterative solution and the RTA, and directional phonon lifetimes in α -P and α -NP.
- [34] X. Wu, V. Varshney, J. Lee, Y. Pang, A. K. Roy, and T. Luo, How to characterize thermal transport capability of 2d materials fairly?—sheet thermal conductance and the choice of thickness, *Chem. Phys. Lett.* **669**, 233 (2017).
- [35] P. Hess, Thickness of elemental and binary single atomic monolayers, *Nanoscale Horiz* **5**, 385 (2020).
- [36] Z. Dai, W. Jin, J.-X. Yu, M. Grady, J. T. Sadowski, Y. D. Kim, J. Hone, J. I. Dadap, J. Zang, R. M. Osgood, Jr., and K. Pohl, Surface buckling of black phosphorus: Determination, origin, and influence on electronic structure, *Phys. Rev. Mater.* **1**, 074003 (2017).
- [37] V. Zólyomi, N. D. Drummond, and V. I. Fal'Ko, Electrons and phonons in single layers of hexagonal indium chalcogenides from ab initio calculations, *Phys. Rev. B* **89**, 205416 (2014).
- [38] H. Şahin, S. Cahangirov, M. Topsakal, E. Bekaroglu, E. Akturk, R. T. Senger, and S. Ciraci, Monolayer honeycomb structures of group-iv elements and iii-v binary compounds: First-principles calculations, *Phys. Rev. B* **80**, 155453 (2009).
- [39] T. Pandey, C. A. Polanco, L. Lindsay, and D. S. Parker, Lattice thermal transport in 1 a 3 c u 3 x 4 compounds (x = p, as, sb, bi): Interplay of anharmonicity and scattering phase space, *Phys. Rev. B* **95**, 224306 (2017).
- [40] M. Christensen, A. B. Abrahamsen, N. B. Christensen, F. Juranyi, N. H. Andersen, K. Lefmann, J. Andreasson, C. R. H. Bahl, and B. B. Iversen, Avoided crossing of rattler modes in thermoelectric materials, *Nat. Mater.* **7**, 811 (2008).
- [41] W. Li, J. Carrete, G. K. H. Madsen, and N. Mingo, Influence of the optical-acoustic phonon hybridization on phonon scattering and thermal conductivity, *Phys. Rev. B* **93**, 205203 (2016).
- [42] M. Zeraati, S. M. V. Allaei, I. A. Sarsari, M. Pourfath, and D. Donadio, Highly anisotropic thermal conductivity of arsenene: An ab initio study, *Phys. Rev. B* **93**, 085424 (2016).
- [43] Y. Kuang, L. Lindsay, S. Shi, X. Wang, and B. Huang, Thermal conductivity of graphene mediated by strain and size, *Int. J. Heat Mass Transf.* **101**, 772 (2016).
- [44] A. Taheri, C. Da Silva, and C. H. Amon, First-principles phonon thermal transport in graphene: Effects of exchange-correlation and type of pseudopotential, *J. Appl. Phys.* **123**, 215105 (2018).
- [45] A. Taheri, C. Da Silva, and C. H. Amon, Highly tunable thermal conductivity of c3n under tensile strain: A first-principles study, *J. Appl. Phys.* **127**, 184304 (2020).
- [46] B. Peng, D. Zhang, H. Zhang, H. Shao, G. Ni, Y. Zhu, and H. Zhu, The conflicting role of buckled structure in phonon transport of 2d group-iv and group-v materials, *Nanoscale* **9**, 7397 (2017).
- [47] S. Lee, S.-H. Kang, and Y.-K. Kwon, Low lattice thermal conductivity of a two-dimensional phosphorene oxide, *Sci. Rep.* **9**, 5149 (2019).
- [48] L. Lindsay, D. A. Broido, and N. Mingo, Flexural phonons and thermal transport in graphene, *Phys. Rev. B* **82**, 115427 (2010).
- [49] L. Zhu, G. Zhang, and B. Li, Coexistence of size-dependent and size-independent thermal conductivities in phosphorene, *Phys. Rev. B* **90**, 214302 (2014).

- [50] W. Li and N. Mingo, Ultralow lattice thermal conductivity of the fully filled skutterudite $\text{YbFe}_4\text{Sb}_{12}$ due to the flat avoided-crossing filler modes, *Phys. Rev. B* **91**, 144304 (2015).
- [51] A. Taheri, C. Da Silva, and C. H. Amon, Phonon thermal transport in $\beta\text{-n}_x$ ($x = \text{p, as, sb}$) monolayers: A first-principles study of the interplay between harmonic and anharmonic phonon properties, *Phys. Rev. B* **99**, 235425 (2019).
- [52] D. L. Nika, E. P. Pokatilov, A. S. Askerov, and A. A. Balandin, Phonon thermal conduction in graphene: Role of umklapp and edge roughness scattering, *Phys. Rev. B* **79**, 155413 (2009).
- [53] X.-J. Ge, K.-L. Yao, and J.-T. Lü, Comparative study of phonon spectrum and thermal expansion of graphene, silicene, germanene, and blue phosphorene, *Phys. Rev. B* **94**, 165433 (2016).